Inorganic Chemistry
Article
pubs.acs.org/IC

Near-IR Luminescence and Field-Induced Single Molecule Magnet of Four Salen-type Ytterbium Complexes

Tian-Qi Liu, Peng-Fei Yan, Fang Luan, Yu-Xin Li, Jing-Wen Sun, Chuan Chen, Fan Yang, Han Chen, Xiao-Yan Zou, and Guang-Ming Li*

Key Laboratory of Functional Inorganic Material Chemistry (MOE); School of Chemistry and Materials Science, Heilongjiang University, Harbin 150080, P. R. China

S *Supporting Information*

ABSTRACT: A series of rigid hexadentate salen-type (H_2L) ytterbium complexes, namely, $[Yb_2L_3(CH_3OH)]\cdot 3CH_3CN$ (**1**), $[Yb_2LL'L''(CH_3OH)(H_2O)_2](ClO_4)_2\cdot CH_3OH\cdot H_2O$ (**2**), $[Yb_2L(OAc)_4(CH_3OH)_2]\cdot 2CH_3OH$ (**3**), and $\{[Yb_2L(OAc)_4]\cdot 3H_2O\}_n$ (**4**) (H_2L = *N*,*N*′-bis(2-oxy-3-methoxybenzylidene)-1,2-phenylenediamine, HL′ = 2-(2′-hydroxy-3′-methyloxy-phenyl)-benzimidazole and HL″ = 3-methoxysalicylaldehyde) have been synthesized by reactions of H_2L with multifarious Yb^{3+} salts. X-ray crystallographic analyses demonstrate that complex **1** is of a triple-decker sandwich-type Yb_2L_3 structure with a ratio of H_2L/Yb = 3:2, **2** and **3** possess the unique Yb_2 core with a ratio of H_2L/Yb = 2:2 and 1:2, respectively, **4** exhibits one dimensional coordination polymers in which the polymeric structures are formed by acetate (OAc^-) groups. All complexes **1**−**4** exhibit near-IR luminescence, which can be rationalized on the basis of the disparate structural effects. The magnetic analysis unveils that all complexes **1**−**4** are of field-induced single-molecule magnet behavior with the energy barriers (U_{eff}/k_B) of 14.5, 2.0, 9.5, and 2.4 K at 3 kOe direct current fields, respectively.

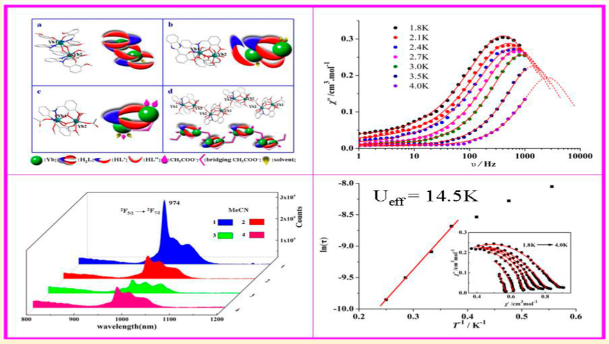

INTRODUCTION

Polynuclear lanthanide complexes continue to attract considerable attentions of distinct luminescent[1] and magnetic properties[2] because of their potential applications in the preparation of new optical,[3] quantum computing,[4] high-density information storage,[5] and molecular spintronics.[6] However, how to control the structures of polynuclear assemblies on the basis of the lanthanide ions is still a challenge since the ions often display high and variable coordination numbers.[1c,7] In recent years, one of the well-known multidentate salen-type ligands has been successfully used to stabilize different lanthanide ions in various coordination environments.[8] In particular, salen-type polynuclear lanthanide complexes have proven to be particularly distinct luminescent complexes[1c,9] and single-molecule magnets (SMMs).[10] Since the first reported the lanthanide SMMs in 2003,[11] much attention has been focused on the magnetic properties and structure of Dy-based[2f,9f,12] and Tb-based[13] complexes. In 2011, Long and co-workers predicted that Yb^{3+} ions can also lead to SMM behavior if employed an appropriate ligand system.[14] In 2012, Yan et al. reported a salen-type and *β*-diketonate complex $[Yb_2(L^1)_2(acac)_2(H_2O)]\cdot 2CH_2Cl_2$ (H_2L^1 = *N*,*N*′-bis(salicylidene)-1,2-phenylenediamine), which exhibits the field-induced SMM behavior with anisotropy barrier of 24.5 K.[15] In 2013, Tong et al. reported a dinuclear Yb-based complex $[Yb_2(H_2cht)_2Cl_4(H_2O)(MeCN)]\cdot MeCN$ (H_2cht = 1,3,5-cyclohexanetriol), of which the anisotropy barrier of Yb_2 complex was 19.5 K.[16] Pointillart et al. presented a redox active dinuclear complex $[Yb(tta)_2(L^3)(L^4)]_2\cdot 1.4(CH_2Cl_2)$ (tta = 2-thenoyltrifluoroacetonate anion, L^3 = 4,5-bis(thiomethyl)-4′-carboxylictetrathiafulvalene and L^4 = 4,5-bis(thiomethyl)-4′-ortho-pyridyl-*N*-oxide-carbamoyltetrathiafulvalene) which exhibits near-IR (NIR) luminescence and single molecule magnetic behavior.[17] It is proved that the Yb^{3+} ion is particularly suitable for bifunction of NIR luminescent and single molecule magnetic complexes.

In view of the recent important progress on the synthesis of the emissive SMMs by using Yb^{3+} ion and salen-type ligand,[15] the rigid hexadentate salen-type ligand of *N*,*N*′-bis(2-oxy-3-methoxybenzylidene)-1,2-phenylenediamine and various ytterbium salts were employed to construct the emissive SMMs of salen-type ytterbium complexes. As a result, a series of salen-type ytterbium complexes with various structures, induced by the various counterions, were isolated. Their NIR luminescent and magnetic properties were studied.

EXPERIMENTAL SECTION

Materials and Instrumentation. The salen-type ligand H_2L[18] and $Yb(acac)_3\cdot H_2O$[19] were synthesized according to the literature. $Yb(ClO_4)_3\cdot 9H_2O$ and $Yb(OAc)_3\cdot 6H_2O$ were prepared by the reactions of Yb_2O_3 and perchloric acid and acetic acid in aqueous solution, respectively. All the other chemicals were obtained from commercial

Received: September 9, 2014
Published: December 11, 2014

Table 1. Crystal Data and Structures Refinement for Complexes 1−4

	1	2	3	4
empirical formula	$C_{73}H_{67}N_9O_{13}Yb_2$	$C_{46}H_{49}N_4O_{22}Cl_2Yb_2$	$C_{34}H_{36}N_2O_{16}Yb_2$	$C_{60}H_{66}N_4O_{27}Yb_4$
formula weight	1624.36	1426.85	1074.73	1967.28
color	buff	buff	buff	buff
crystal system	orthorhombic	monoclinic	triclinic	orthorhombic
space group	*Pbca*	$P2_1/c$	$P\bar{1}$	$P2_12_12_1$
a (Å)	20.194(5)	22.254(5)	11.620(5)	13.734(3)
b (Å)	24.610(5)	15.400(3)	12.541(5)	16.582(3)
c (Å)	26.983(5)	21.218(4)	14.103(5)	17.723(4)
α (deg)	90.000(5)	90	89.023(5)	90
β (deg)	90.000(5)	114.68(3)	68.562(5)	90
γ (deg)	90.000(5)	90	86.208(5)	90
V (Å^3)	13 410(5)	6607(2)	1908.8(13)	4036.0(14)
Z	8	4	2	2
ρ_{calcd} (g cm^{-3})	1.599	1.179	1.870	1.678
μ (mm^{-1})	2.844	2.858	4.943	4.669
F(000)	6416	2288	1044	1980
R_1,^{a} [$I > 2\sigma$ (I)]	0.0312	0.0542	0.0254	0.0338
wR_2,^{b} [$I > 2\sigma$ (I)]	0.0682	0.1373	0.0582	0.0675
R_1,^{a} (all data)	0.0476	0.1107	0.0305	0.0445
wR_2,^{b} (all date)	0.0779	0.1559	0.0610	0.0698
GOF on F^2	1.169	0.882	1.033	0.990

$^a R_1 = \sum||F_0| - |F_c||/|F_0|$. $^b wR_2 = [\sum w(F_0^2 - F_c^2)^2/\sum w(F_0^2)^2]^{1/2}$

sources and used without further purification. Fourier transform infrared (FT-IR) data (Supporting Information, Figure S1) were recorded on a PerkinElmer 100 spectrophotometer in the region 4000−500 cm^{-1} using KBr disks. UV−vis spectra (in CH_3CN) (Supporting Information, Figure S2) were recorded on a PerkinElmer Lambda 35 spectrometer. Elemental (C, N, and H) analysis were carried out on a PerkinElmer 2400 analyzer. Thermal analyses (Supporting Information, Figure S3) were carried out on a PerkinElmer STA 6000 in the temperature region of 30−800 °C with a heating rate of 10 °C min^{-1} under atmosphere. Powder X-ray diffraction (PXRD) data (Supporting Information, Figure S5) were recorded on a Rigaku D/Max-3B X-ray diffractometer with Cu Kα radiation, the scanning rate was 4°/s, 2θ ranging from 5−50°. Near-IR emission spectra and luminescence lifetimes of complexes **1**−**4** were measured with an Edinburgh FLS 920 fluorescence spectrophotometer and a single photon counting spectrometer from Edinburgh Instruments (FLS 920) with a microsecond pulse lamp as the excitation, respectively. The magnetic susceptibility for complexes **1**−**4** was measured with a Quantum Design MPMS XL-7 SQUID-VSM magnetometer. The magnetic corrections were made by using Pascal's constants.

Synthesis of [$Yb_2L_3(CH_3OH)$]·$3CH_3CN$ (1). A solution of $Yb(acac)_3$·H_2O (0.4 mmol) in CH_3OH (10 mL) was added to a solution of H_2L (0.6 mmol) in CH_3CN (25 mL). The mixture was stirred under ambient temperature for 12 h. Then, diethyl ether was diffused slowly into the solution. Yellow crystals of **1** were obtained in about two week. Yield: 0.2130 g (66.5%). Elemental analysis (%) calcd for $C_{73}H_{67}N_9O_{13}Yb_2$ (1624.36): C, 53.97; H, 4.16; N, 7.76. found: C, 53.90; H, 4.16; N, 7.75; IR (KBr, cm^{-1}): 3414(m), 1615(s), 1472(m), 1246(s), 1196(m), 741(m). UV−vis [MeOH, λ]: 239, 298, 386 nm.

Synthesis of [$Yb_2LL'L''(CH_3OH)(H_2O)_2$]($ClO_4$)$_2$·$CH_3OH$·$H_2O$ (2). A solution of $Yb(ClO_4)_3$·$9H_2O$ (0.30 mmol) in CH_3OH (10 mL) was added to a solution of H_2L (0.3 mmol) in CH_2Cl_2 (10 mL). The mixture was stirred under ambient temperature for 8 h. The color of the mixture turned from orange to brown. Then, diethyl ether was diffused slowly into the solution. Yellow crystals of **2** were obtained in ca. one month. Yield: 0.1431 g (66.2%). Elemental analysis (%) calcd for $C_{46}H_{49}N_4O_{22}Cl_2Yb_2$ (1426.88): C, 38.72; H, 3.46; N, 3.93. found: C, 38.71; H, 3.44; N, 3.91; IR (KBr, cm^{-1}): 3387(m), 2946(w), 1617(s), 1446(s), 1235(m), 1098(m), 962(m), 741(m). UV−vis [MeOH, λ]: 230, 301, 394 nm.

Synthesis of [$Yb_2L(OAc)_4(CH_3OH)_2$]·$2CH_3OH$ (3). Triethylamine (10 mL of 0.1 M CH_2Cl_2 solution) was added to a solution of H_2L (0.2 mmol) and $Yb(OAc)_3$·$6H_2O$ (0.4 mmol) in CH_3OH (10 mL). The mixture was stirred under ambient temperature for 12 h. The color of the mixture turned from orange to luminous yellow. Then, diethyl ether was diffused slowly into the solution. Yellow crystals of **3** were obtained in ca. one week. Yield: 0.1348 g (62.8%). Elemental analysis (%) calcd for $C_{34}H_{36}N_2O_{16}Yb_2$ (1074.43): C, 38.00; H, 3.38; N, 2.61. found: C, 38.00; H, 3.37; N, 2.60; IR (KBr, cm^{-1}): 3386(m), 2930(w), 1614(s), 1555(vs), 1237(m), 1200(m), 970(m), 739(w). UV−vis [MeOH, λ]: 237, 300, 379 nm.

Synthesis of {[$Yb_2L(OAc)_4$]·$3H_2O$}$_n$ (4). Triethylamine (10 mL of 0.1 M CH_2Cl_2 solution) was added to a solution of H_2L (0.2 mmol) and $Yb(OAc)_3$·$6H_2O$ (0.6 mmol) in CH_3OH (10 mL). The mixture was stirred under ambient temperature for 12 h. The color of the mixture turned from orange to luminous yellow. Then, diethyl ether was diffused slowly into the solution. Yellow crystals of **4** were obtained in ca. one week. Yield: 0.1233 g (62.7%). Elemental analysis (%) calcd for $C_{60}H_{66}N_4O_{27}Yb_4$ (1967.28): C, 36.63; H, 3.38; N, 2.85. found: C, 36.61; H, 3.36; N, 2.82; IR (KBr, cm^{-1}): 3309(m), 1615(s), 1554(vs), 1459(s), 1238(w), 1197(w), 756(w), 744(w). UV−vis [MeOH, λ]: 237, 300, 380 nm.

X-ray Crystallography. Suitable single crystals of complexes **1**−**4** were selected on a Rigaku R-AXIS RAPID. All data were collected on a Siemens SMART CCD diffractometer with graphite-monochromated Mo Kα (λ = 0.710 73 Å) at room temperature. Empirical absorption corrections based on equivalent reflections were applied. The structures of complexes **1**−**4** were solved by direct methods, and all non-hydrogen atoms were anisotropically refined by full-matrix least-squares methods on F^2 with using SHELXS-97 crystallographic software package.[20] The crystal data and structure refinement details were summarized in Table 1 for complexes **1**−**4**. Additional crystallographic information is available in the Supporting Information.

■ RESULTS AND DISCUSSION

Structural Descriptions of Complexes 1−4. X-ray crystallographic analysis reveals that complex **1** crystallizes in an orthorhombic space group of *Pbca*. As shown in Figure 1a, complex **1** contains three ligands, two Yb^{3+} ions, and one methanol molecule. The Yb1^{3+} ion is octacoordinated by two N_2O_2 sets of the top and middle salen-type ligands exhibiting a square antiprism geometry with D_{4d} point group (Supporting Information, Figure S4a). The Yb2^{3+} ion is also octacoordinated by the N_2O_2 set of the bottom ligand and three O atoms from the common salen-type ligand and one methanol molecule displaying a bicapped trigonal prism geometry with C_{2v} point group (Supporting Information, Figure S4a). The two Yb^{3+} ions are bridged by the phenolic O7 and O8 atoms from the common salen-type ligand with the Yb1···Yb2 distance of 3.8570 Å, the Yb−O bond lengths are in the range of 2.161−2.844 Å, and the Yb−N bond lengths are in the range of 2.447−2.530 Å, which is in accordance with the reported data.[21] Notably, complex **1** has a typical triple-decker dinuclear sandwich structure with the ratio of H_2L/Yb = 3:2. It is similar to the reported triple-decker dinuclear sandwich complexes $[Yb_2(L^5)_3(CHOH)]_3·0.5H_2O$ (H_2L^5 = *N*,*N*′-bis(salicylidene)-1,2-(phenylenediamine))[22] and $[Dy_2(L^6)_3(CHOH)]_3$ (H_2L^6 = *N*,*N*′-bis(salicylidene)-1,2-cyclohexanediamine)[10g] but differs in the coordination numbers of the lanthanide ions in which one of the Dy^{3+} ions is heptacoordinated, while the Yb^{3+} ions were octacoordinated by an extra methoxy group in complex **1**.

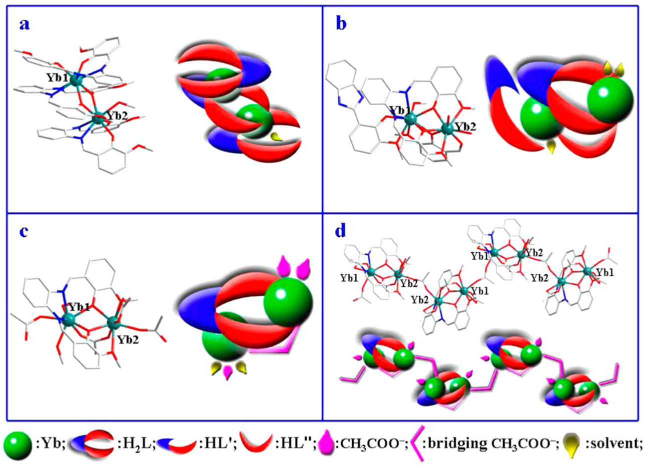

Figure 1. Structures and the schematic illustrations of **1** (a), **2** (b), **3** (c), and **4** (d).

X-ray crystallographic analysis reveals that complex **2** is a discrete neutral complex with a unique Yb$_2$ core, crystallizing in a triclinic space group of $P\bar{1}$ and containing three different ligands, namely, H_2L, HL′ (2-(2′-hydroxy-3′-methyloxyphenyl)benzimidazole), and HL″ (3-methoxysalicylaldehyde). HL′ and HL″ are supposed to result from the decomposition of H_2L in the environment of ClO_4^- anions (Supporting Information, Scheme S1). The positive charges of the cations $[Yb_2LL'L'']^{2+}$ in complex **2** are balanced by two ClO_4^- anions. In the structure of complex **2** (Figure 1b), the Yb1^{3+} ion is nine-coordinated by the N_2O_2 pocket of the H_2L, four O atoms from the hydroxy and methoxy groups of the other two ligands of HL′ and HL″, as well as one O atom from one methanol molecule, forming the triangular dodecahedron geometry with D_{3h} point group (Supporting Information, Figure S4b). The Yb2^{3+} ion is octacoordinated to the O_2O_2 set of the H_2L ligand, two O atoms from one hydroxy group and one aldehyde group of the ligand (HL″) as well as two O atoms from two water molecule, respectively, forming a bicapped trigonal prism geometry with C_{2v} point group (Supporting Information, Figure S4b). The two Yb^{3+} ions are bridged by the phenolate O1, O3, and O6 atoms with a distance of 3.8570 Å. The Yb−O bond lengths are in the range of 2.229−2.769 Å and the Yb−N bond lengths are 2.474 to 2.486 Å. Notably, complex **2** is distinctively different from the reported salen-type dinuclear complex of $[Dy_2L^7(H_2L^7)(teaH_2)(o\text{-vanillin})(H_2O)](ClO_4)_2·2CH_3OH·H_2O$ (teaH$_2$ = triethanolamine, H_2L^7 = *N*,*N*′-bis(3-methoxysalicylidene)-1,2-cyclohexanediamine) although both of them have the same bridging ligand (o-vanillin).[23] For complex **2** the two Yb^{3+} ions are in the N_2O_2 and O_2O_2 pocket of one H_2L ligand and coordinated by the decomposition H_2L ligand (HL′ and HL″), one methanol molecule and two water molecule with the ratio of H_2L/Yb = 2:2. In contrast to the metal centers of two Dy^{3+} ions in complex $[Dy_2L^7(H_2L^7)(teaH_2)(o\text{-vanillin})(H_2O)](ClO_4)_2·2CH_3OH·H_2O$,[23] one is in the inner salen-type N_2O_2 coordination pocket of the L^{2-} ligand, and the other is chelated by a teaH$_2^-$ ligand.

X-ray crystallographic analysis reveals that complex **3** is a discrete ionic complex with a similar dinuclear Yb$_2$ core as that in complex **2**, crystallizing in a triclinic space group of $P\bar{1}$ and containing two Yb^{3+} ions, one ligand, four acetate anions, and two methanol molecules. In the structure of complex **3** (Figure 1c), the Yb1^{3+} ion is octacoordinated by the N_2O_2 set of the ligand and four O atoms from one bridging, one terminal acetate group, and two methanol molecules, respectively, exhibiting a square antiprism geometry with D_{4d} point group (Supporting Information, Figure S4c). The Yb2^{3+} ion is also octacoordinated by the O_2O_2 set of the ligand and four O atoms from one terminal, one bridging and one bidentate acetate group, displaying a bicapped trigonal prism geometry with C_{2v} point group (Supporting Information, Figure S4c). The two Yb^{3+} ions are bridged by the phenolate O7 and O8 atoms as well as an acetate group with a distance of 3.6961 Å. Obviously, the bridging acetate group may responsible for stabilizing the dinuclear Yb$_2$ core. The Yb−O bond lengths are in the range of 2.199−2.524 Å, and those of Yb2−N1 and Yb2−N2 are 2.454 and 2.465 Å, respectively. Noticeably, to the best of our knowledge complex **3** represents the first example of the hexadentate salen-type homodinuclear lanthanide complex in which one ligand captured two Yb^{3+} ions with the ratio of H_2L/Yb = 1:2 although numerous salen-type dinuclear lanthanide complexes have been reported. It may result from the tension of the lanthanide ions in the two pockets arising from the steric inhibition.

X-ray crystallographic analysis reveals that complex **4** crystallizes in an orthorhombic space group of $P2_12_12_1$ with a one dimensional (1D) coordination polymer structure. The positive charges of two Yb^{3+} cations are balanced by one L^{2-} and four acetate anions. A view of the structure unit of **4** is shown in Figure 1d. Each Yb$_2$ unit in complex **4** is almost the same as that of complex **3**, however one acetate group bidentate bridges between two dinuclear unit as a linker to form a 1D chain structure in complex **4**. In comparison with **3** the two Yb^{3+} ions are also octacoordinated forming a square antiprism geometry and a bicapped trigonal prism geometry with D_{4d} and C_{2v} point group (Supporting Information, Figure S4d), respectively, while the two methanol molecules are substituted by one bidentate acetate group. The Yb−O bond lengths are in the range of 2.192−2.543 Å and the bond lengths of Yb2−N1 and Yb2−N2 are 2.412 and 2.445 Å, respectively, which is longer than previously reported $[Yb_2(L^8)_2(OAc)_2(MeOH)_2]_n$ (H_2L^8 = *N,N′*-ethylene bis(salicylideneimine)) complex.[24] Although both complex **4** and $[Yb_2(L^8)_2(OAc)_2(MeOH)_2]_n$ are alike in terms of the compositions and dinuclear structure, they are distinguished from the ratio of H_2L/Yb. For example, the ratio of H_2L/Yb is 2:2 for complex $[Yb_2(L^8)_2(OAc)_2(MeOH)_2]_n$, while the ratio of H_2L/Yb is 1:2 for complex **4** in which the two Yb^{3+} ions are in the cavities of N_2O_2 and O_2O_2 of one ligand, respectively.

To further distinguish the structures of complexes **1**−**4**, the dinuclear cores and local coordination geometry are showed in Figure 2 and Supporting Information, Figure S4. For complexes **1**, **2**, and **3**, the two Yb^{3+} ions are coordinated by three ligands, two ligands, and one ligand with the ratio of H_2L/Yb = 3:2, 2:2, and 1:2, respectively. Moreover, the two Yb^{3+} ions are bridged by two phenolate oxygen from the same salen-type ligand. The dihedral angles between the two triangle planes (Yb1O7O8 and Yb2O7O8) is 178.962°, 137.017°, 154.171°, and 153.011°, as well as the two Yb^{3+} ions are 3.8570, 3.4874, 3.6961, and 3.6630 Å for complexes **1**−**4**, respectively. Obviously, the larger the dihedral angles, the longer the distance of the two Yb^{3+} ions. Noticeably, these structure parameters such as the ratio of H_2L/Yb, the dihedral angle, and distances between two Yb^{3+} ions will play essential roles on NIR luminescence and magnetic properties of complexes **1**−**4**.

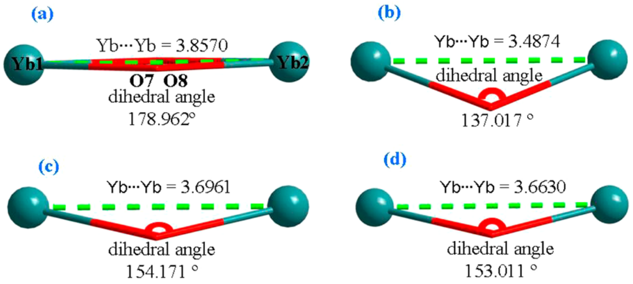

Figure 2. Distance and the dihedral angle between two Yb^{3+} ions in complexes **1** (a), **2** (b), **3** (c), and **4** (d).

Structural Diversity and Effect of Anions. On the basis of the above descriptions and discussions, the diversiform anions dominate the structure of complexes **1**−**4**. For example, the structure of **1** with a ratio of H_2L/Yb = 3:2 results from the weak coordination ability of acac⁻ anion in which the acac⁻ anion is not involved in the coordination. While the H_2L ligand decomposes to the HL′ and HL″ in the environment of $Yb(ClO_4)_3{\cdot}9H_2O$ (Supporting Information, Scheme S1) in complex **2**. Since the ClO_4^- anion do not participate in the coordination of Yb^{3+} ions playing a charge-balancing role, which provides an opportunity for the H_2L, HL′, and HL″ ligands to coordination of the Yb^{3+} ions, which leads to the structure of **2** with a ratio of H_2L/Yb = 2:2. In contrast, the coordination ability of the OAc⁻ anions is stronger than that of the acac⁻ and ClO_4^- anions so that it is easy to participate in the coordination. Thus, when the ligand reacts with $Yb(OAc)_3{\cdot}6H_2O$ forming a dinuclear complex **3**, which contains four OAc⁻ anions for Yb^{3+} ions with the ratio of H_2L/Yb = 1:2. However, increasing in the ratio of OAc⁻ anion in complex **4**, it bridges between the two dinuclear units as a linker to form a 1D chain structure in complex **4**.

NIR Luminescence. The free ligand H_2L exhibits absorption bands at 223, 279, and 331 nm in CH_3CN (Supporting Information, Figure S2). Once the coordination occurs, the UV−vis spectra of complexes **1**−**4** reveal similar ligand-centered bands near 230−239, 298−301, and 379−394 nm, which are red-shifted in comparison with that of the free ligand. The NIR photoluminescence spectra of **1**−**4** are recorded with the excited wavelength of 412 nm in the CH_3CN (1×10^{-5} M) solution at room temperature. NIR photoluminescence spectra of **1**−**4** exhibit the typical NIR emission bands of Yb^{3+} ion that could be observed at 974, 1006, and 1033 nm, respectively (Figure 3). The emission at 974 nm is assigned to the $^2F_{5/2}{\rightarrow}^2F_{7/2}$ transition. Notably, the NIR emission of Yb^{3+} ion in **1**−**4** is not a sharp transition but appears as a series of bands with two other broad bands centered at 1006 and 1033 nm. A similar phenomenon, observed in a previous report, is attributed to the stark splitting or crystal-field.[25] Notice that the NIR luminescence intensity of the Yb^{3+} ion for complex **1** is much stronger than that of complexes **2**−**4**. It supports the idea that the three ligands in complex **1** provide an improved shield on Yb^{3+} ion and forbid the attachment of acetate anions and the solvent molecules that may partially quench the lanthanide luminescence. Although complexes **2**−**4** have the same number of Yb^{3+} ions, which may provide the same number of emissive centers,[26] plenty of coordinated solvent molecules and acetate anions will quench the NIR luminescence of the Yb^{3+} ions that lack encapsulation.[27] Thus, complex **3** exhibits the weakest NIR luminescent intensity among complexes **1**−**4**, which has two coordinated solvent CH_3OH molecules and four coordinated acetate anions.

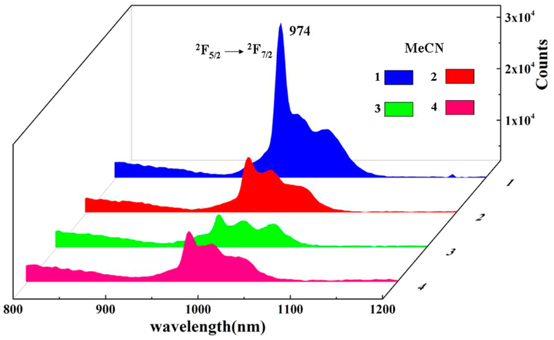

Figure 3. NIR emission spectra of **1**−**4** in CH_3CN (1×10^{-5} M) at room temperature.

To further investigate the NIR luminescence, we also measured the time-resolved luminescence decay responses of complexes **1**−**4** in the NIR region by using the time-correlated single photon counting (TCSPC) technique. As shown in Figure 4, the lifetime of complexes **1**−**4** has a satisfactory fit to a monoexponential lifetime, and the lifetime for **1** is the longest among complexes **1**−**4**. The intrinsic luminescence quantum yield of the Ln^{3+} ions may be estimated by $\Phi_{Ln} = \tau_{obs}/\tau_0$ in which τ_{obs} is the observed emission lifetime and τ_0 is the radiative or "natural lifetime", specifically, 2.0 ms for the Yb^{3+} ion.[26] Thus, the maximum estimated NIR quantum yield for complexes **1**−**4** lies in the range of 0.4−0.6% (Table 2). It is higher than that of the reported salen-type dinuclear ytterbium complex $[Yb(H_2L)_2(NO_3)]_2{\cdot}CH_2Cl_2$,[1d] but lower than that of complex $[Yb(H_2L)_2(NO_3)]_2(PF_6)_4{\cdot}4H_2O{\cdot}2CH_2Cl_2$[1d] due to the shielding for Yb^{3+} ions of the four ligands in complex $[Yb(H_2L)_2(NO_3)]_2(PF_6)_4{\cdot}4H_2O{\cdot}2CH_2Cl_2$[1d] (Table 2).

Magnetic Properties. Magnetic measurements for **1**−**4** were performed on polycrystalline samples. The phase purity of

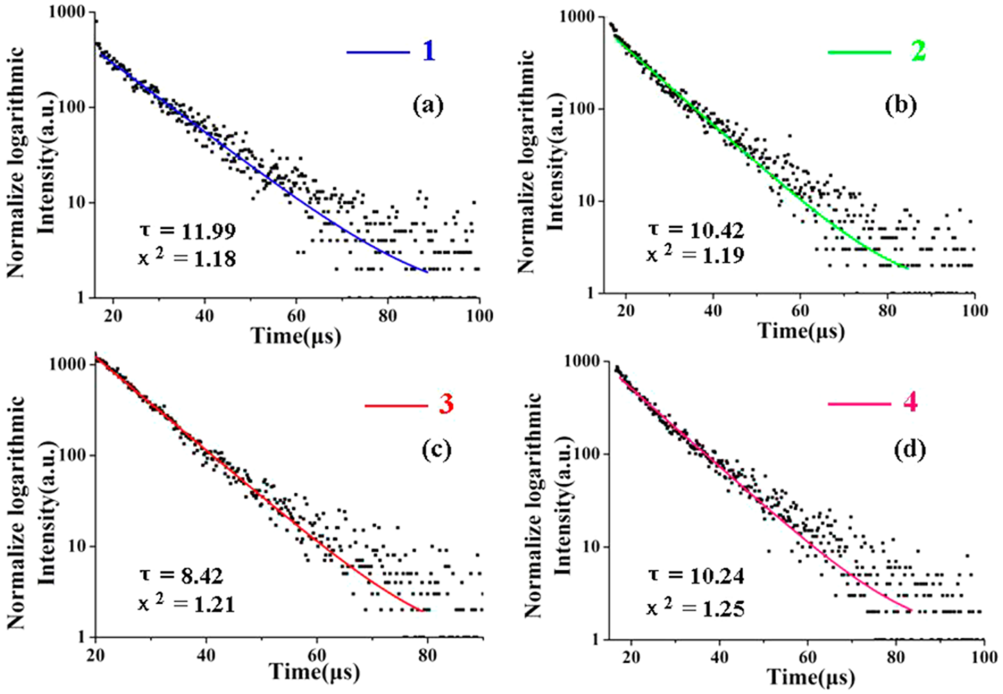

Figure 4. Luminescence decay profiles for complexes **1** (a), **2** (b), **3** (c), and **4** (d) in CH_3CN solution at 298 K.

Table 2. NIR Luminescent Lifetime and the Intrinsic Luminescence Quantum Yield of Complexes 1−4

complexes	τ (μS)	Φ_{Ln} (%)
1	11.99	0.600
2	10.42	0.515
3	8.42	0.421
4	10.24	0.512
$[Yb(H_2L)_2(NO_3)]_2(PF_6)_4 \cdot 4H_2O \cdot 2CH_2Cl_2$[1d]	18.31	0.916
$[Yb\ (H_2L)_2(NO_3)]_2 \cdot CH_2Cl_2$[1d]	5.1	0.255

the bulk samples was verified by XRD analyses (Supporting Information, Figure S5). The temperature dependence of the $\chi_M T$ product is shown in Figure 5 and Supporting Information, Figure S6. The value of $\chi_M T$ is 5.29, 4.80, 5.38, and 5.35 cm^3 K mol^{-1} at 300 K under 1 kOe field for complexes **1−4**, respectively, which are close to the expected theoretical values 5.14 cm^3 K mol^{-1} for two noninteracting Yb^{3+} ions ($^2F_{7/2}$, $S = 1/2$, $J = 7/2$, $g = 8/7$, $C = 2.57$ cm^3 K mol^{-1}). When the samples cooled, the $\chi_M T$ product gradually decreased to reach a minimum value of 1.72, 2.46, 1.32, and 2.2 cm^3 K mol^{-1} at 2.0 K for **1−4**, respectively, which is mostly due to the thermal depopulation of the Stark sublevels and/or significant magnetic anisotropy in Yb^{3+} ion systems.[2e,28] The field dependence of the magnetization for complexes **1−4** rises slowly before reaching 3.4, 3.5, 3.3, and 3.4 N μ_B at 2.0 K, respectively. Moreover, the absence of a superposition of the M versus H data at higher field indicates the presence of significant magnetic anisotropy in complexes **1−4**.[15]

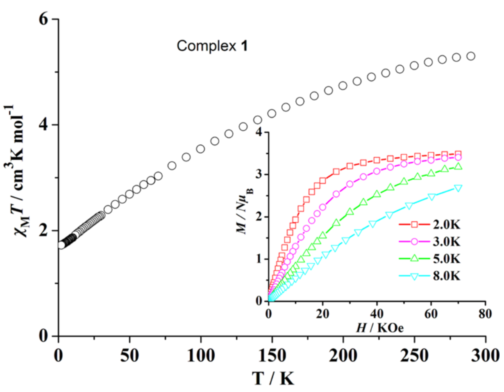

Figure 5. Temperature dependence of $\chi_m T$ at 1 kOe field for **1**. (inset) The field dependence of magnetization for **1** at 2.0−8.0 K.

Alternating current (ac) susceptibility curves at zero external field show no out-of-phase signal (χ'') of the ac susceptibility at frequencies up to 1000 Hz and the temperatures down to 1.8 K for complexes **1−4**. It suggests that the magnetization relaxation time (τ) is much shorter than 1/2 $\pi\nu$ and that the quantum tunnelling of the magnetization (QTM) plays an important role.[29] However, when a static direct current (dc) field of 3 kOe is applied, the χ'' component is strongly enhanced indicating that the presence of QTM can be significantly reduced by the applied field.[30] Indeed, the temperature- and frequency-dependent ac susceptibility signal were observed at lower temperatures, indicative of feld-induced SMM behavior for complexes **1−4** (Figure 6 and 7 and Supporting Information, Figures S7 and S8), while the peak of out-phase signal (χ'') only could be observed for complexes **1** (Figure 6 left) and **3** (Figure 7 left) at low temperature. Moreover, for **1** (Figure 6, right) and **3** (Figure 7, right) the relaxation time (τ) between 1.8 and 4 K was estimated by fitting the χ'' versus frequency curves.[30b,c] On the basis of the Arrhenius relation [$\tau = \tau_0 \exp(U_{eff}/k_B T)$], the energy barriers ($U_{eff}/k_B$) are 14.5 and 9.5 K for **1** (Figure 6 right) and **3** (Figure 7 right), respectively, with the pre-exponential factors (τ_0) of 1.6×10^{-6} s and 4.8×10^{-6} s. In addition, Cole−Cole plots can be fitted to the generalized Debye model (α_{Cole} = 0.009−0.297 and 0.067−0.363 for **1** (Figure 6, left inset) and **3** (Figure 7, left insert), respectively, based on the ac susceptibility measure-

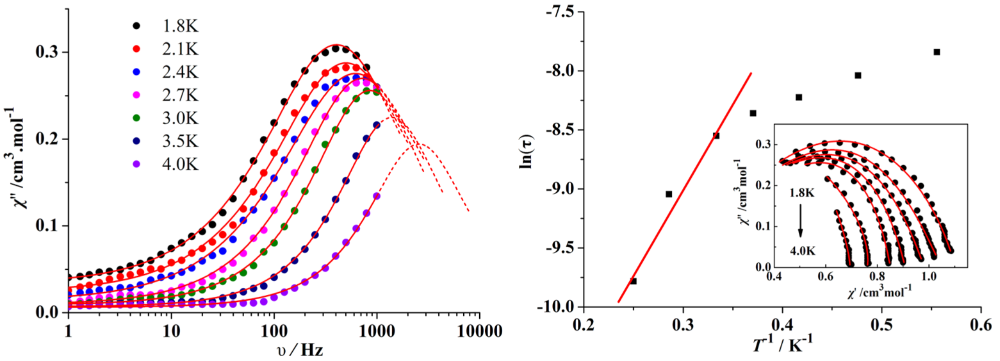

Figure 6. (left) Frequency dependence of the out-of-phase component of the ac susceptibility under 3 kOe dc field for **1**. The red lines are the best fits obtained with the generalized Debye model. All data were well-simulated with α value of less than 0.23. (right) Magnetization relaxation time, $\ln(t)$ vs $1/T$ for **1** under 3 kOe dc field. The red line is fitted with the Arrhenius law. (inset) Cole–Cole (α = 0.009–0.297) plots at the temperatures indicated.

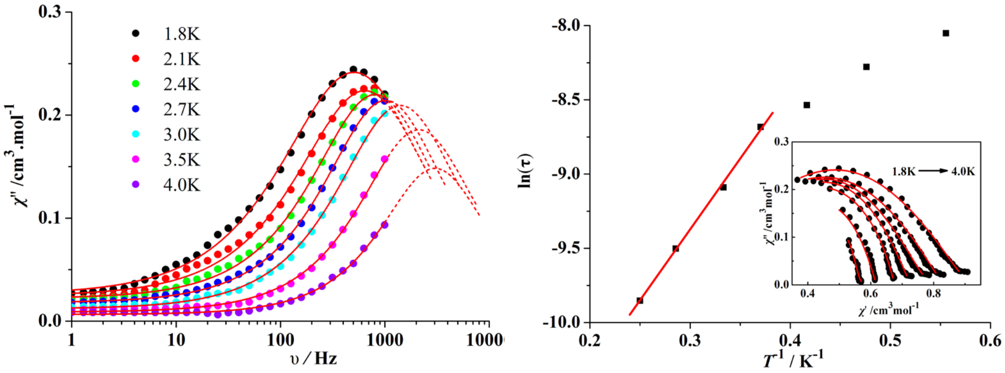

Figure 7. (left) Frequency dependence of the out-of-phase component of the ac susceptibility under 3 kOe dc field for **3**. The red lines are the best fits obtained with the generalized Debye model. All data were well-simulated with α value of less than 0.23. (right) Magnetization relaxation time, $\ln(t)$ vs $1/T$ for **3** under 3 kOe dc field. The red line is fitted with the Arrhenius law. (inset) Cole–Cole (α = 0.067–0.363) plots at the temperatures indicated.

ments.[31] It indicates that a single relaxation is mainly involved in the present relaxation process.

When a static field of 3 kOe was applied, complexes **2** and **4** displayed clear frequency-dependent out-of-phase (χ'') signals at low temperatures, but also show no peak of the in-phase signal (χ') and the out-of-phase signal (χ''). Thus, energy barrier and relaxation time cannot be obtained by Arrhenius equation. By way of assuming a single relaxation process, the Debye model and equation $\ln(\chi''/\chi') = \ln(\omega\tau_0) + E_a/k_BT$[23,32] yield the best-fitting results, which provide an energy barrier (U_{eff}/k_B) of 2.0 and 2.4 K for **2** (Supporting Information, Figure S7 right) and **4** (Supporting Information, Figure S8 right), respectively, with the pre-exponential factors (τ_0) of 3.7 × 10^{-5} s and 1.0 × 10^{-5} s. Obviously, the energy barriers of complexes **1**–**4** are lower than those reported for analogous dinuclear ytterbium complexes; for example, the U_{eff} values of complexes $[Yb_2(L^1)_2(acac)_2(H_2O)]\cdot 2CH_2Cl_2$,[15] $[Yb_2(H_2cht)_2Cl_4(H_2O)(MeCN)]\cdot MeCN$,[16] and $[Yb(tta)_2(L^3)(L^4)]_2\cdot 1.4(CH_2Cl_2)$[17] are 24.5 K (1600 Oe), 19.5 K (3500 Oe), and 21.2 K (2000 Oe), respectively, which are attributed to the distinctly different ligand fields. However, in comparison with pure salen-type Dy SMMs, far fewer pure salen-type Yb SMMs have been reported. To the best of our knowledge, complex **4** is the first reported salen-type ytterbium SMM with 1D chain structure.

It is known that the slow relaxation of the magnetization for lanthanide SMMs is closely related to crystal field symmetry and 4f ions anisotropy.[33] Among complexes **1**, **3**, and **4** with the same coordination symmetric Yb^{3+} ions, complex **1** exhibits the highest energy barrier (Table 3), which is possibly attributed to the larger dihedral angle between the two triangle planes and to the longer distances between the two Yb^{3+} ions in complex **1** than those for complexes **3** and **4**. Thus, the smallest dihedral angle between the two triangle planes and the shortest distances result in the lowest energy barrier of complex **2**. Further, it again demonstrates that the slight differences in terms of dihedral angle, coordination symmetry, and the distance of the lanthanide ions may affect the nature of single-axial anisotropy of the lanthanide ions through the single-axial ligand-field symmetry and therefore generate the different dynamic magnetic behavior for **1**–**4**.[34]

Table 3. Energy Barrier (U_{eff}/k_B) and Comparison of the Structural Data for 1–4

	1	2	3	4
U_{eff}/k_B (K)	14.5	2.0	9.0	2.4
dihedral angle between the two triangle plane (deg)	178.962	137.017	154.171	153.011
distance of two Yb^{3+} ions (Å)	3.8570	3.4874	3.6961	3.6630
coordination symmetries (Yb1/Yb2)	D_{4d}/C_{2v}	D_{3h}/C_{2v}	D_{4d}/C_{2v}	D_{4d}/C_{2v}

■ CONCLUSIONS

We have synthesized a series of ytterbium complexes with distinct structures by the reaction of *N*,*N*′-bis(2-oxy-3-methoxybenzylidene)-1,2-phenylenediamine with multifarious Yb^{3+} salts. It suggests that the rigid hexadentate salen-type ligand and the anions play essential roles in modulating the structures. The size of the Yb^{3+} ion dominates the formation of the salen-type dinuclear complexes **3** and **4** with the ratio of the ligand/Yb = 1:2, which are seldom reported. NIR luminescent analysis again demonstrates that the coordinated solvents and the shielding of the ligand on Yb^{3+} ions dominate the NIR emission intensity and the intrinsic quantum yields. The magnetic analysis for complexes **1**−**4** reveals that the ligand field of *N*,*N*′-bis(2-oxy-3-methoxybenzylidene)-1,2-phenylenediamine is able to induce the magnetic relaxations of the Yb^{3+} ions, and the dihedral angle, distance, and the coordination geometry of the two Yb^{3+} ions for complexes **1**−**4** may affect the single-axial anisotropy of the Yb^{3+} ion, which results in the different energy barriers.

■ ASSOCIATED CONTENT

Ⓢ Supporting Information

Schematic iIllustration of decomposition of H_2L, FT-IR spectra, UV spectra, TG-DSC curves, magnetic data, coordination geometry of Yb^{3+}, XRD patterns, temperature dependence of $\chi_{\mathrm{m}}T$, and X-ray crystallographic files (CIF) for **1**−**4**. This material is available free of charge via the Internet at http://pubs.acs.org. CCDC Nos. 1012920, 1012921, 1012922, and 91012919 contain the supplementary crystallographic data for complexes **1**−**4**, respectively. These data can be obtained free of charge from the Cambridge Crystallographic Data Center via www.ccdc.cam.ac.uk/data_request/cif.

■ AUTHOR INFORMATION

Corresponding Author

*E-mail: gmli_2000@163.com. Fax: 86-451-86673647.

Notes

The authors declare no competing financial interest.

■ ACKNOWLEDGMENTS

This work is financially supported by the National Natural Science Foundation of China (Nos. 51272069, 21471051, and 51402092).

■ REFERENCES

(1) (a) Binnemans, K. *Chem. Rev.* **2009**, *109*, 4283−4374. (b) Bünzli, J.-C. G.; Eliseeva, S. V. *J. Rare Earths* **2010**, *28*, 824−842. (c) Liao, S.; Yang, X.; Jones, R. A. *Cryst. Growth Des.* **2012**, *12*, 970−974. (d) Zou, X.; Y, P.; Zhang, J.; Zhang, F.; Hou, G.; Li, G. *Dalton Trans.* **2013**, *42*, 13190−13199.

(2) (a) Habib, F.; Brunet, G.; Vieru, V.; Korobkov, I.; Chibotaru, L. F.; Murugesu, M. *J. Am. Chem. Soc.* **2013**, *135*, 13242−13245. (b) Nakano, M.; Oshio, H. *Chem. Soc. Rev.* **2011**, *40*, 3239−3248. (c) Sorace, L.; Benelli, C.; Gatteschi, D. *Chem. Soc. Rev.* **2011**, *40*, 3092−3104. (d) Woodruff, D. N.; Winpenny, R. E.; Layfield, R. A. *Chem. Rev.* **2013**, *113*, 5110−5148. (e) Zhang, H.; Lin, S. Y.; Xue, S.; Wang, C.; Tang, J. *Dalton Trans.* **2014**, *43*, 6262−6268. (f) Ungur, L.; Le Roy, J. J.; Korobkov, I.; Murugesu, M.; Chibotaru, L. F. *Angew. Chem., Int. Ed.* **2014**, *53*, 4413−4417.

(3) (a) Artizzu, F.; Mercuri, M. L.; Serpe, A.; Deplano, P. *Coord. Chem. Rev.* **2011**, *255*, 2514−2529. (b) Katkova, M. A.; Bochkarev, M. N. *Dalton Trans.* **2010**, *39*, 6599−6612.

(4) Liu, J. L.; Wu, J. Y.; Chen, Y. C.; Mereacre, V.; Powell, A. K.; Ungur, L.; Chibotaru, L. F.; Chen, X. M.; Tong, M. L. *Angew. Chem., Int. Ed.* **2014**, *53*, 12966−12970.

(5) Bogani, L.; Wernsdorfer, W. *Nat. Mater.* **2008**, *7*, 179−186.

(6) Woodruff, D. N.; Winpenny, R. E.; Layfield, R. A. *Chem. Rev.* **2013**, *113*, 5110−5148.

(7) Yang, X.; Jones, R. A.; Huang, S. *Coord. Chem. Rev.* **2014**, *273*−*274*, 63−75.

(8) Dalla Cort, A.; De Bernardin, P.; Forte, G.; Mihan, F. Y. *Chem. Soc. Rev.* **2010**, *39*, 3863−3874.

(9) (a) Feng, W.; Zhang, Y.; Zhang, Z.; Lu, X.; Liu, H.; Shi, G.; Zou, D.; Song, J.; Fan, D.; Wong, W. K.; Jones, R. A. *Inorg. Chem.* **2012**, *51*, 11377−11386. (b) Gao, T.; Yang, Y.; Sun, W.-B.; Li, G.-M.; Hou, G.-F.; Yan, P.-F.; Li, J.-T.; Ding, D.-D. *CrystEngComm* **2013**, *15*, 6213. (c) Yang, X.; Oye, M. M.; Jones, R. A.; Huang, S. *Chem. Commun.* **2013**, *49*, 9579−9581. (d) Yang, X.; Jones, R. A.; Wong, W. K. *Chem. Commun.* **2008**, 3266−3268. (e) Feng, W.; Zhang, Y.; Lü, X.; Hui, Y.; Shi, G.; Zou, D.; Song, J.; Fan, D.; Wong, W.-K.; Jones, R. A. *CrystEngComm* **2012**, *14*, 3456.

(10) (a) Lin, P. H.; Burchell, T. J.; Clerac, R.; Murugesu, M. *Angew. Chem., Int. Ed.* **2008**, *47*, 8848−8851. (b) Lin, P. H.; Burchell, T. J.; Ungur, L.; Chibotaru, L. F.; Wernsdorfer, W.; Murugesu, M. *Angew. Chem., Int. Ed.* **2009**, *48*, 9489−9492. (c) Lin, P. H.; Sun, W. B.; Yu, M. F.; Li, G. M.; Yan, P. F.; Murugesu, M. *Chem. Commun.* **2011**, *47*, 10993−10995. (d) Sun, W.-B.; Han, B.-L.; Lin, P.-H.; Li, H.-F.; Chen, P.; Tian, Y.-M.; Murugesu, M.; Yan, P.-F. *Dalton Trans.* **2013**, *42*, 13397−13403. (e) Yan, P. F.; Lin, P. H.; Habib, F.; Aharen, T.; Murugesu, M.; Deng, Z. P.; Li, G. M.; Sun, W. B. *Inorg. Chem.* **2011**, *50*, 7059−7065. (f) Yang, F.; Yan, P.; Li, Q.; Chen, P.; Li, G. *Eur. J. Inorg. Chem.* **2012**, *2012*, 4287−4293. (g) Zhu, J.; Song, H.-F.; Yan, P.-F.; Hou, G.-F.; Li, G.-M. *CrystEngComm* **2013**, *15*, 1747−1752.

(11) Ishikawa, N.; Sugita, M.; Ishikawa, T.; Koshihara, S.-y.; Kaizu, Y. *J. Am. Chem. Soc.* **2003**, *125*, 8694−8695.

(12) (a) Gavey, E. L.; Beldjoudi, Y.; Rawson, J. M.; Stamatatos, T. C.; Pilkington, M. *Chem. Commun.* **2014**, *50*, 3741−3743. (b) Jia, L.; Chen, Q.; Meng, Y. S.; Sun, H. L.; Gao, S. *Chem. Commun.* **2014**, *50*, 6052−6055. (c) Katoh, K.; Asano, R.; Miura, A.; Horii, Y.; Morita, T.; Breedlove, B. K.; Yamashita, M. *Dalton Trans.* **2014**, *43*, 7716−7725. (d) Shen, S.; Xue, S.; Lin, S. Y.; Zhao, L.; Tang, J. *Dalton Trans.* **2013**, *42*, 10413−10416. (e) Guo, Y. N.; Ungur, L.; Granroth, G. E.; Powell, A. K.; Wu, C.; Nagler, S. E.; Tang, J.; Chibotaru, L. F.; Cui, D. *Sci. Rep. (U.K.)* **2014**, *4*, 5471. (f) da Cunha, T. T.; Jung, J.; Boulon, M. E.; Campo, G.; Pointillart, F.; Pereira, C. L.; Le Guennic, B.; Cador, O.; Bernot, K.; Pineider, F.; Golhen, S.; Ouahab, L. *J. Am. Chem. Soc.* **2013**, *135*, 16332−16335. (g) Guo, P. H.; Liu, J. L.; Jia, J. H.; Wang, J.; Guo, F. S.; Chen, Y. C.; Lin, W. Q.; Leng, J. D.; Bao, D. H.; Zhang, X. D.; Luo, J. H.; Tong, M. L. *Chem.—Eur. J.* **2013**, *19*, 8769−8773. (h) Guo, P. H.; Meng, Y.; Chen, Y. C.; Li, Q. W.; Wang, B. Y.; Leng, J. D.; Bao, D. H.; Jia, J. H.; Tong, M. L. *J. Mater. Chem. C* **2014**, *2*, 8858−8864.

(13) (a) Branzoli, F.; Carretta, P.; Filibian, M.; Zoppellaro, G.; Graf, M. J.; Galan-Mascaros, J. R.; Fuhr, O.; Brink, S.; Ruben, M. *J. Am. Chem. Soc.* **2009**, *131*, 4387−4396. (b) Lodi Rizzini, A.; Krull, C.; Balashov, T.; Mugarza, A.; Nistor, C.; Yakhou, F.; Sessi, V.; Klyatskaya, S.; Ruben, M.; Stepanow, S. *Nano Lett.* **2012**, *12*, 5703−5707. (c) Inose, T.; Tanaka, D.; Tanaka, H.; Ivasenko, O.; Nagata, T.; Ohta, Y.; De Feyter, S.; Ishikawa, N.; Ogawa, T. *Chem.—Eur. J.* **2014**, *20*, 11362−11369.

(14) Rinehart, J. D.; Long, J. R. *Chem. Sci.* **2011**, *2*, 2078−2085.

(15) (a) Lin, P. H.; Sun, W. B.; Tian, Y. M.; Yan, P. F.; Ungur, L.; Chibotaru, L. F.; Murugesu, M. *Dalton Trans.* **2012**, *41*, 12349−12352. (b) Liu, J. L.; Yuan, K.; Leng, J. D.; Ungur, L.; Wernsdorfer, W.; Guo, F. S.; Chibotaru, L. F.; Tong, M. L. *Inorg. Chem.* **2012**, *51*, 8538−8544.

(16) Leng, J. D.; Liu, J. L.; Zheng, Y. Z.; Ungur, L.; Chibotaru, L. F.; Guo, F. S.; Tong, M. L. *Chem. Commun.* **2013**, *49*, 158−160.

(17) Pointillart, F.; Le Guennic, B.; Golhen, S.; Cador, O.; Maury, O.; Ouahab, L. *Chem. Commun.* **2013**, *49*, 615−617.

(18) Koner, R.; Lee, G. H.; Wang, Y.; Wei, H. H.; Mohanta, S. *Eur. J. Inorg. Chem.* **2005**, *2005*, 1500−1505.

(19) Stites, J. G.; McCarty, C.; Quill, L. L. *J. Am. Chem. Soc.* **1948**, *70*, 3142−3143.

(20) Sheldrick, G. M. *Acta Crystallogr., Sect. A: Found. Crystallogr.* **2007**, *64*, 112−122.

(21) Wang, H.; Liu, C.; Liu, T.; Zeng, S.; Cao, W.; Ma, Q.; Duan, C.; Dou, J.; Jiang, J. *Dalton Trans.* **2013**, *42*, 15355−15360.

(22) Yan, P.-F.; Chen, S.; Chen, P.; Zhang, J.-W.; Li, G.-M. *CrystEngComm* **2011**, *13*, 36.

(23) Zhang, L.; Zhang, P.; Zhao, L.; Lin, S.-Y.; Xue, S.; Tang, J.; Liu, Z. *Eur. J. Inorg. Chem.* **2013**, *2013*, 1351−1357.

(24) Yang, X.; Jones, R. A.; Rivers, J. H.; Wong, W. K. *Dalton Trans.* **2009**, 10505−10510.

(25) Kang, T. S.; Harrison, B. S.; Bouguettaya, M.; Foley, T. J.; Boncella, J. M.; Schanze, K. S.; Reynolds, J. R. *Adv. Funct. Mater.* **2003**, *13*, 205−210.

(26) He, H.; Zhu, X.; Hou, A.; Guo, J.; Wong, W.-K.; Wong, W.-Y.; Li, K.-F.; Cheah, K.-W. *Dalton Trans.* **2004**, 4064−4073.

(27) (a) Feng, W.; Zhang, Y.; Lü, X.; Hui, Y.; Shi, G.; Zou, D.; Song, J.; Fan, D.; Wong, W.-K.; Jones, R. A. *CrystEngComm* **2012**, *14*, 3456−3463. (b) Richardson, F. S. *Chem. Rev.* **1982**, *82*, 541−552.

(28) (a) Long, J.; Habib, F.; Lin, P. H.; Korobkov, I.; Enright, G.; Ungur, L.; Wernsdorfer, W.; Chibotaru, L. F.; Murugesu, M. *J. Am. Chem. Soc.* **2011**, *133*, 5319−5328. (b) Li, Q. W.; Liu, J. L.; Jia, J. H.; Leng, J. D.; Lin, W. Q.; Chen, Y. C.; Tong, M. L. *Dalton Trans.* **2013**, *42*, 11262−11270. (c) Joarder, B.; Mukherjee, S.; Xue, S.; Tang, J.; Ghosh, S. K. *Inorg. Chem.* **2014**, *53*, 7554−7560.

(29) Liu, J. L.; Yuan, K.; Leng, J. D.; Ungur, L.; Wernsdorfer, W.; Guo, F. S.; Chibotaru, L. F.; Tong, M. L. *Inorg. Chem.* **2012**, *51*, 8538−8544.

(30) (a) Gao, Y.; Zhao, L.; Xu, X.; Xu, G.-F.; Guo, Y.-N.; Tang, J.; Liu, Z. *Inorg. Chem.* **2011**, *50*, 1304−1308. (b) Poneti, G.; Bernot, K.; Bogani, L.; Caneschi, A.; Sessoli, R.; Wernsdorfer, W.; Gatteschi, D. *Chem. Commun.* **2007**, 1807−1809. (c) Xue, S.; Zhao, L.; Guo, Y. N.; Tang, J. *Dalton Trans.* **2012**, *41*, 351−353.

(31) (a) Aubin, S. M.; Sun, Z.; Pardi, L.; Krzystek, J.; Folting, K.; Brunel, L.-C.; Rheingold, A. L.; Christou, G.; Hendrickson, D. N. *Inorg. Chem.* **1999**, *38*, 5329−5340. (b) Cole, K. S.; Cole, R. H. *J. Chem. Phys.* **1941**, *9*, 341−351. (c) Guo, Y. N.; Xu, G. F.; Guo, Y.; Tang, J. *Dalton Trans.* **2011**, *40*, 9953−9963.

(32) (a) Lin, S.-Y.; Zhao, L.; Guo, Y.-N.; Zhang, P.; Guo, Y.; Tang, J. *Inorg. Chem.* **2012**, *51*, 10522−10528. (b) Mazarakioti, E. C.; Poole, K. M.; Cunha-Silva, L.; Christou, G.; Stamatatos, T. C. *Dalton Trans.* **2014**, *43*, 11456−11460. (c) Adhikary, A.; Sheikh, J. A.; Biswas, S.; Konar, S. *Dalton Trans.* **2014**, *43*, 9334−9343.

(33) (a) Gao, F.; Cui, L.; Liu, W.; Hu, L.; Zhong, Y. W.; Li, Y. Z.; Zuo, J. L. *Inorg. Chem.* **2013**, *52*, 11164−11172. (b) Gao, F.; Yao, M.-X.; Li, Y.-Y.; Li, Y.-Z.; Song, Y.; Zuo, J.-L. *Inorg. Chem.* **2013**, *52*, 6407−6416. (c) Gonidec, M.; Luis, F.; Vílchez, À.; Esquena, J.; Amabilino, D. B.; Veciana, J. *Angew. Chem., Int. Ed.* **2010**, *49*, 1623−1626. (d) Hanninen, M. M.; Mota, A. J.; Aravena, D.; Ruiz, E.; Sillanpaa, R.; Camon, A.; Evangelisti, M.; Colacio, E. *Chem.—Eur. J.* **2014**, *20*, 8410−8420.

(34) Yao, M. X.; Zheng, Q.; Gao, F.; Li, Y. Z.; Song, Y.; Zuo, J. L. *Dalton Trans.* **2012**, *41*, 13682−13690.